# Landslide Susceptibility Mapping using AI-driven Geospatial Analysis, Remote Sensing and Geophysical Validation: A Case Study of the Manolo Fortich Hydro Power Plant

Glimpse Bagayas
Center for Structural Engineering and Informatics, MSU - Iligan Institute of Technology

Joel Opon
Center for Structural Engineering and Informatics, MSU - Iligan Institute of Technology

https://doi.org/10.5109/7395579

出版情報：Proceedings of International Exchange and Innovation Conference on Engineering & Sciences (IEICES). 11, pp.624-631, 2025-10-30. International Exchange and Innovation Conference on Engineering & Sciences
バージョン：

# Landslide Susceptibility Mapping using AI-driven Geospatial Analysis, Remote Sensing and Geophysical Validation: A Case Study of the Manolo Fortich Hydro Power Plant

Glimpse Bagayas[1], Joel Opon[1,2,3]
[1] Center for Structural Engineering and Informatics, MSU – Iligan Institute of Technology, Iligan City
[2] Research Institute for Engineering and Innovative Technology, MSU – Iligan Institute of Technology
[3] Department of Civil Engineering and Technology, MSU – Iligan Institute of Technology
* Corresponding author email: glimpse.bagayas@g.msuiit.edu.ph

**Abstract:** *Landslides present a significant geohazard risk to hydropower infrastructure. This study integrates AI-driven geospatial analysis, remote sensing, and geophysical surveys to develop an enhanced landslide susceptibility mapping framework for the Manolo Fortich 1 Hydroelectric Power Plant (MF1 HEPP) in Bukidnon, Philippines. Using Slide3 AI software, InSAR, photogrammetry, and Electrical Resistivity Tomography (ERT), the study improves landslide risk predictions. First-pass AI detected 101 critical slope segments, which were refined to 83 after field validation and a second pass. Model accuracy improved, with the Area Under the Curve (AUC) rising from 0.85 to 0.91, and classification accuracy increasing from 84.42% to 91.77%. The results demonstrate that AI-based geotechnical analysis, coupled with geophysical validation, enhances prediction accuracy and reduces false positives. These findings highlight the importance of digital twin modeling in hydropower risk assessment and infrastructure resilience.*

**Keywords:** Landslide Susceptibility, Artificial Intelligence, Remote Sensing, Geophysical Survey, Risk Mitigation

## 1. INTRODUCTION

With the global push for renewable energy, hydropower plants are increasingly constructed in geologically unstable regions, where landslides pose a major threat to infrastructure stability [1, 20, 33]. Steep terrains and unstable slopes exacerbate the risk of failure, leading to severe operational disruptions, financial losses, and safety hazards [15, 30]. As an example, the Manolo Fortich 1 Hydropower Plant, a critical energy facility in the Philippines, has incurred Php 671 million in restoration costs and Php 871 million in endangered assets due to landslides. As extreme weather events increase, improving landslide susceptibility mapping with AI-driven methodologies becomes essential for infrastructure resilience and long-term sustainability [14]. Landslide susceptibility mapping (LSM) relies on evaluating key conditioning factors such as slope gradient, soil properties, hydrology, land cover, and seismic activity [2, 4]. Traditional methods, including the analytic hierarchy process (AHP) and frequency ratio (FR) models, assign weighted factors to these elements, generating susceptibility zones based on historical data [8, 16, 24, 31]. However, these methods suffer from limitations, such as subjectivity in factor weighting, difficulty incorporating real-time data, and inconsistent prediction accuracy across different geological conditions [7, 9, 32].

More advanced deterministic models, such as the limit equilibrium method (LEM) and finite element method (FEM), attempt to improve precision by computing factor of safety (FoS) values for slope stability [17, 22, 27]. These approaches, however, are highly data-intensive, requiring detailed geotechnical surveys that may not be feasible for large-scale applications [14, 25]. Moreover, their inability to dynamically adjust to climate variability and hydrological changes limits their predictive reliability [18, 29].

On the other hand, recent advances in AI, remote sensing, and geophysical validation, are also utilized in landslide susceptibility; but there remains several gaps in application. These include limited AI adaptation to extreme climate variability, which hinders real-time adjustments to changing precipitation patterns and affects prediction accuracy [4, 5]. Traditional models also often lack high-resolution 3D slope stability capabilities, making it difficult to capture complex geological conditions in large-scale hydropower projects [6, 21]. Furthermore, few studies integrate AI, remote sensing, and geophysical validation into a unified framework for infrastructure risk assessment [3, 11].

This paper presents an AI-driven, multi-pass landslide susceptibility mapping approach that integrates AI-based slope stability analysis using *Slide3* software, geophysical validation through electrical resistivity tomography (ERT) and standard penetration tests (SPT), and GIS-based spatial classification for comprehensive landslide risk assessment. *Slide3* is a 3D slope stability modeling software developed by Rocscience, capable of simulating complex terrain geometries, slip surfaces, and soil profiles using Limit Equilibrium Methods. In this study, Slide3 is enhanced with particle swarm optimization (PSO) and non-uniform rational basis spline (NURBS) surfaces were employed to enhance the accuracy of critical slip surface identification [6, 9]. The paper focuses on the Manolo Fortich 1 Hydroelectric Power Plant (MF1 HEPP) in Bukidnon, Philippines as a case study for the method—an area prone to landslides due to its steep topography, high rainfall, and seismic activity [20, 25]. Incorporating the AI-driven Slide3 modeling, geophysical validation could improve slope failure predictions, ultimately enhancing hydropower risk mitigation strategies [12, 22].

## 2. METHODOLOGY

### 2.1 Research design

This study employs a multi-disciplinary approach integrating AI-based geospatial modeling, remote

sensing, and geophysical validation to develop an advanced landslide susceptibility mapping framework. The workflow consists of three key phases (Figure 1):

1. AI-Driven Initial Landslide Detection – *Slide3* software applies machine learning algorithms to identify critical slip surfaces based on InSAR-derived deformation data and digital elevation models (DEMs).
2. Geophysical Validation – Field reconnaissance, electrical resistivity tomography (ERT), and standard penetration test (SPT) data verify subsurface conditions and slope stability parameters.
3. Refinement of Susceptibility Maps – A second-pass, a more refine and detailed AI analysis integrates ERT, SPT and photogrammetry to create a high resolution digital twin model to enhance the accuracy of critical slip failure – Slide3 software is used to perform 3D slope stability analysis, generating Factor of Safety (FoS) maps that guide GIS-based zoning of susceptibility levels. By combining AI predictions (PSO and NURBS) with engineering-based (Janbu and Bishop Method) slope simulations from Slide3, the model produces more accurate and geotechnically-informed susceptibility maps [4, 10, 22].

This structured approach ensures a high-precision landslide prediction model tailored for hydropower infrastructure resilience [19].

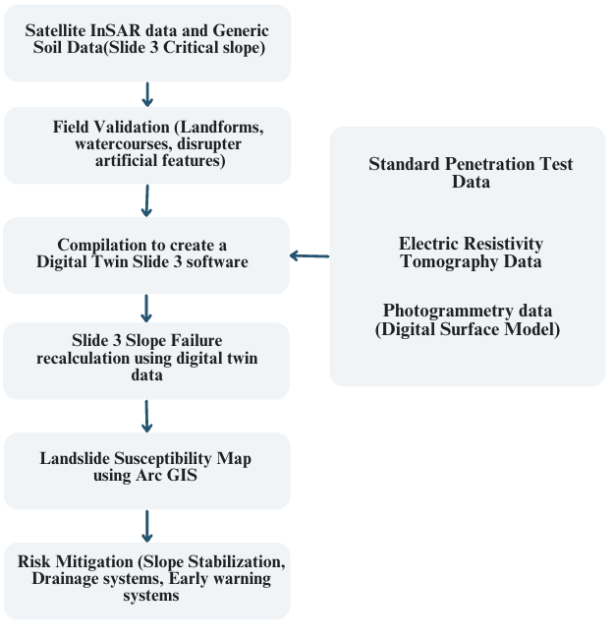


Fig. 1 Conceptual Framework

## 2.2 Study area

The Manolo Fortich 1 Hydroelectric Power Plant (MF1 HEPP) is located in Manolo Fortich, Bukidnon, Philippines (Figure 2). The site features steep to moderate slopes and rugged terrain, with key infrastructure strategically positioned along riverbanks, particularly at the confluence of the Guihean and Amusig rivers, which flow into the Tagoloan River (Figure 3. Accessibility is limited due to the absence of road networks. The area is covered with grasses, shrubs, and trees, while the bedrock consists mainly of metamorphic schists and igneous rocks [29]. The region falls under a Type III climate, with a wet season from May to November and a dry season from December to April [25].

Although Bukidnon is outside the main typhoon belt, extreme weather events like Typhoon Bopha (2012) and Typhoon Rai (2021) emphasize the need for geohazard assessments [29].

MF1 HEPP is vulnerable to landslides, seismic activity, flooding, and volcanic hazards. Landslides pose significant risks to penstocks, pipelines, and embankments, especially during earthquakes. The site's proximity to the Tagoloan Fault (~6 km southwest) increases susceptibility to seismic-induced slope failures.


Fig. 2 Location map of the Manolo Fortich Hydro Power Plant 1

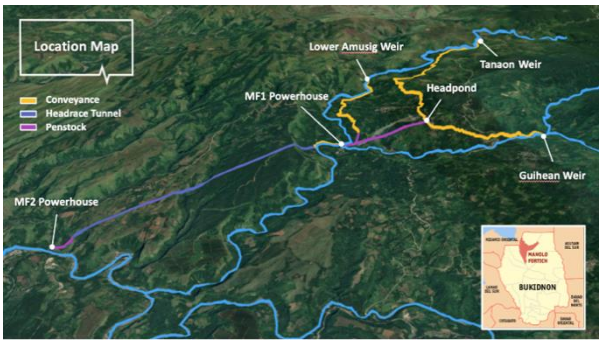


Fig. 3 Location map of the Manolo Fortich Hydro Power Plant 1

## 2.3 Data collection methods

Remotely sensed data includes InSAR satellite imagery shown in Figure 4 and photogrammetry data shown in Figure 5, which detects ground deformation and slope movement, and photogrammetry, generating high-resolution digital surface models (DSM) for terrain analysis [7, 9, 22, 23, 26, 28,].

Fig. 4 Slide 3 built in satellite InSAR data (TRE ALTAMIRA)

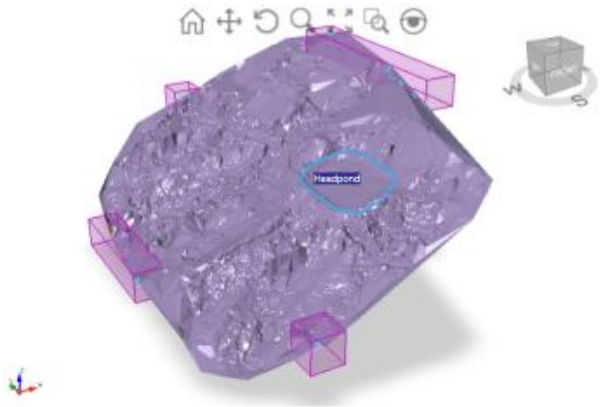


Fig. 5 Slide 3 Photogrammetry data processed of TB 90-92

Geophysical data acquisition comprises ERT shown in Figure 6 for identifying subsurface weaknesses and slip surfaces and Standard Penetration Tests (SPT) for assessing soil strength and liquefaction potential [30, 9, 28, 22, 26].

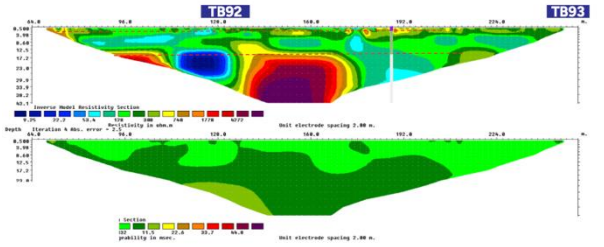


Fig. 6 Electrical resistivity tomography of TB 92-93

### 2.4 Data processing and analysis

Two analytical passes with per performed for the acquired data. The first-pass landslide detection is conducted using AI-based slope stability assessment in *Slide3* software, integrating InSAR [35] displacement data, DEMs, and soil properties to calculate Factor of Safety (FoS) values. Field validation is performed through on-site inspections that verify predicted landslide-prone areas based on geotechnical and environmental indicators such as slip scarps, soil deformation, and hydrological anomalies. A Digital Twin Model in Figure 7 is created by integrating DSM, ERT, and SPT data to refine slope stability predictions through computational analysis.

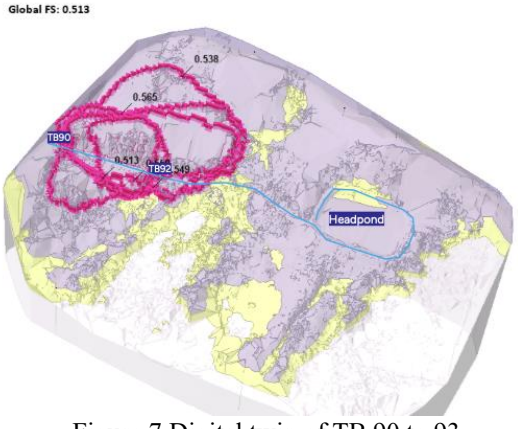


Figure 7 Digital twin of TB 90 to 93

The second pass landslide detection phase refines the AI-driven assessment by incorporating high-resolution photogrammetry and subsurface geophysical data, using Janbu and Bishop slope stability models for improved accuracy [9, 13, 22, 28, 30].

## 3.0 RESULTS AND DISCUSSION

### 3.1 First-pass AI prediction

The first pass with the utilization of the *Slide3* software outputs the preliminary landslide susceptibility analysis, identifying 101 critical slope segments based on Factor of Safety (FoS) values shown in Figure 8 [34].

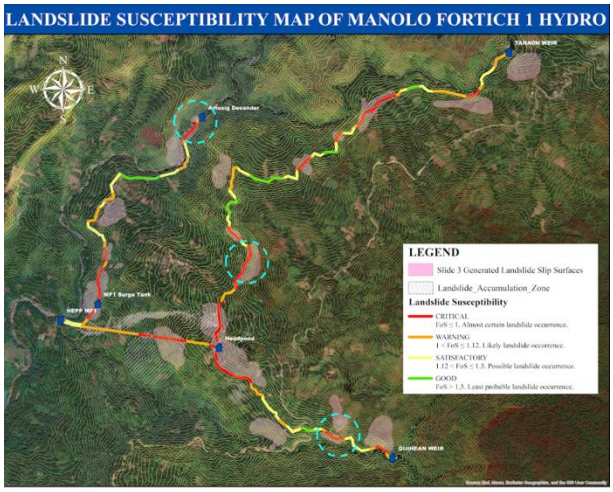


Fig. 8 First pass landslide susceptibility map output using satellite data

The highest-risk zones were located in Tanaon (TB 78-86), Guihean (TB 12-18), and Upper Amusig (TB 4-9). Of these, 15 areas required immediate mitigation due to infrastructure vulnerability. The initial classification was validated using historical landslide data, site validation and satellite imagery, risk assessment and mitigation. The key findings are summarized in Table 1. Table 1 presents first-pass AI model results, detailing classification metrics that assess its initial accuracy in identifying landslide-prone and stable slope areas.

Table 1. Summary of high-risk landslide areas predicted by slide 3 software (first pass) and risk mitigation status

| Area (Thrust Blocks) | No. of Area Predicted as Critical Slope | Risk Mitigation Status |
|---|---|---|
| Tanaon 0-1 | 2 | Completed |
| Tanaon 10-13 | 4 | Completed |
| Tanaon 19-24 | 6 | Completed |
| Tanaon 31-34 | 4 | Completed |
| Tanaon 41-44 | 4 | Completed |
| Tanaon 55-60 | 6 | Completed |
| Tanaon 72-76 | 5 | Completed |
| Tanaon 78-86 | 9 | No mitigation |
| Tanaon 91-96 | 6 | In Progress |
| Guihean 0-4 | 5 | Completed |
| Guihean 12-18 | 7 | Completed |

| Area (Thrust Blocks) | No. of Area Predicted as Critical Slope | Risk Mitigation Status |
|---|---|---|
| Guihean 30-33 | 4 | Completed |
| Guihean 47-55 | 9 | Completed |
| High Head 5-10 | 6 | No mitigation |
| Upper Amusig 0-9 | 10 | Completed |
| Upper Amusig 25-29 | 5 | Completed |
| Upper Amusig 38-40 | 3 | Completed |
| Upper Amusig 43-48 | 6 | Completed |
| **Total** | **101Areas** | |

### 3.2 Second pass AI refinement

To improve predictive accuracy, a second pass analysis was conducted using high-resolution photogrammetry and ERT data, the second pass model refined the risk classification in Table 2, reducing high-risk areas from 101 to 83 shown in Figure 9, indicating improved classification reliability. The first-pass analysis provided an essential preliminary screening of 101 critical slopes using remote sensing and AI. In contrast, the second-pass refinement, guided by ERT, SPT, and photogrammetry, reduced the number of critical slopes to 83, improved classification accuracy, and better supported the implementation of targeted slope stabilization and drainage strategies in unmitigated zones such as TB78, TB92, and High Head TB 5-7 areas.

To optimize processing and resource allocation, our focus is on areas that lack mitigation measures and are currently undergoing implementation, including Tanaon TB 78-82, TB 91-95, High Head Penstock TB 5-7, and High Head Pond Areas.

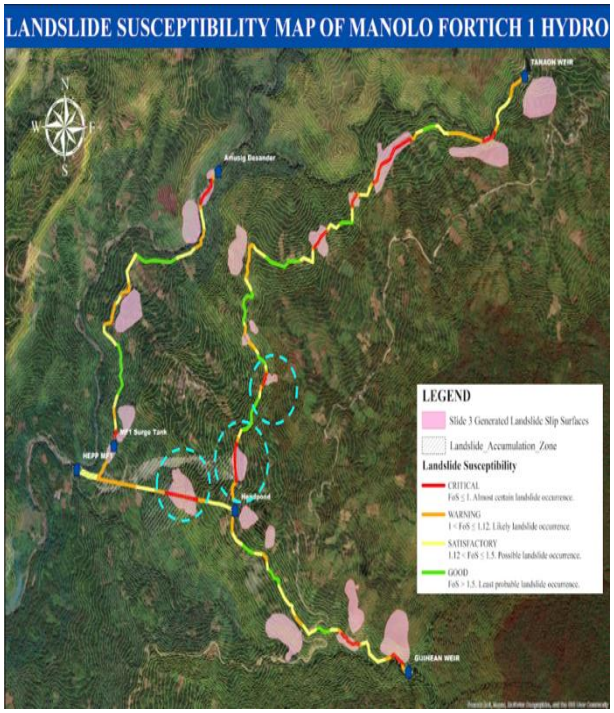


Fig. 9 Second pass landslide susceptibility map output using digital twin model

Table 2. Summary of high-risk landslide areas predicted by slide 3 software (Second pass) and risk mitigation status

| Area (Thrust Blocks) | Area Predicted as Critical Slope | Risk Mitigation Status |
|---|---|---|
| Tanaon 0-1 | 2 | Completed |
| Tanaon 10-13 | 4 | Completed |
| Tanaon 19-24 | 6 | Completed |
| Tanaon 31-34 | 4 | Completed |
| Tanaon 41-44 | 4 | Completed |
| Tanaon 55-60 | 6 | Completed |
| Tanaon 72-74 | 3 | Completed |
| Tanaon 78-82 | 5 | No mitigation |
| Tanaon 91-95 | 5 | In Progress |
| Guihean 0-4 | 5 | Completed |
| Guihean 12-18 | 7 | Completed |
| Guihean 30-33 | 4 | Completed |
| Guihean 47-48 | 2 | Completed |
| Guihean 53-55 | 3 | Completed |
| High Head 5-7 | 3 | No mitigation |
| Upper Amusig 0-1 | 2 | Completed |
| Upper Amusig 4-9 | 6 | Completed |
| Upper Amusig 25-29 | 5 | Completed |
| Upper Amusig 38-40 | 3 | Completed |
| Upper Amusig 45-48 | 4 | Completed |
| **Total** | **83 Areas** | |

### 3.3 Model performance improvement

The integration of photogrammetry and ERT provided enhanced subsurface characterization. Comparative analysis of Bishop and Janbu slope stability methods shown in Figure 10 (a) and (b), respectively, demonstrated significant convergence in failure surface predictions, reducing false positives from 26 to 9 and improving overall accuracy from 84.42% of the first pass to 91.77% of the second pass.

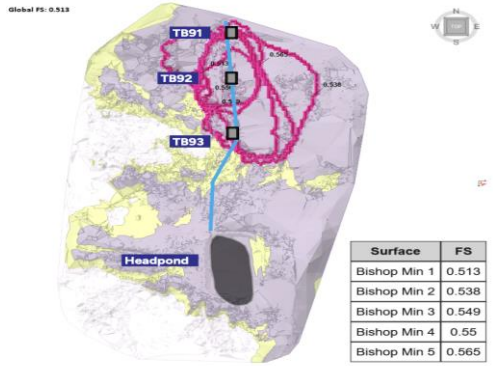


(a) Bishop Method

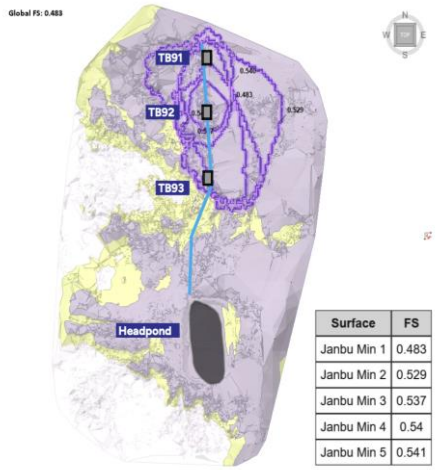


(b) Janbu Method

Fig. 10 Second critical slip failure of Bishop (a) and Janbu (b)

The results of the landslide susceptibility mapping demonstrate a significant improvement in predictive accuracy between the first and second pass analyses, as reflected in the Figure 10 shown an increased area under the curve (AUC) values in the receiver operating characteristic (ROC) curve and enhanced classification metrics.

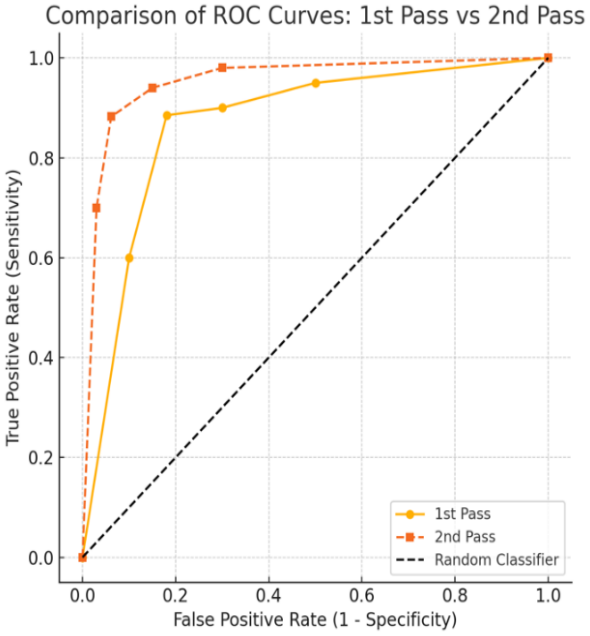


Fig. 10 AUC RUC Curve comparison for 1st and 2nd pass

The first-pass analysis, which relied primarily on remote sensing techniques and general soil data, yielded an AUC value of 0.85—classified as a very good model (0.8–0.9 range shown in Table 3)—with an overall accuracy of 84.42% (TP = 77, TN = 118, FP = 26, FN = 10). While the second pass analysis AUC value increased to 0.91, placing it within the excellent model performance range shown in Table 3 (0.9–1.0), while accuracy rose to 91.77% (TP = 75, TN = 137, FP = 9, FN = 10), with a substantial reduction in false positives, enhancing the model's ability to distinguish stable from unstable areas.

Table 3 Classification for interpreting the AUC of the ROC curve based on accuracy and performance

| AUC Value | Interpretation | Model Performance |
|---|---|---|
| 0.90 - 1.00 | Excellent | Highly accurate model |
| 0.80 - 0.89 | Very Good | Strong discrimination |
| 0.70 - 0.79 | Fair | Moderate discrimination |
| 0.60 - 0.69 | Poor | Weak discrimination |
| 0.50 - 0.59 | Fail / Random Guessing | No discrimination |
| 0.5 | No Better Than Random | Useless model |

The results of first pass and second pass are comparatively presented in Table 4. The first pass approach lacked the depth to fully capture complex subsurface conditions influencing slope stability, leading to a relatively high false positive rate and some underestimation of landslide hazards. In contrast, the second pass analysis incorporated additional geophysical datasets, including soil properties and Electrical Resistivity Tomography (ERT) data, resulting in a refined digital twin model that improved classification accuracy. The improved predictive capability of the second pass analysis has critical implications for landslide risk mitigation, as a more accurate susceptibility map—validated against historical landslide and risk mitigation implemented data in true positive (TP) classes—provides a stronger foundation for site-specific interventions such as slope stabilization, optimized drainage systems, and early warning mechanisms. The transition from very good to excellent model performance underscores the importance of a multi-phase analytical approach, where initial broad-scale predictions are refined using additional geophysical and AI-driven iterative processing. Future passes could further enhance the model by integrating real-time monitoring data, including rainfall intensity, soil moisture fluctuations, and ground displacement sensors, to dynamically update susceptibility predictions based on evolving environmental conditions.

Table 4 Classification Model Performance Comparison

| Analysis | First Pass | Second Pass |
|---|---|---|
| True Positive (TP) | 77 | 75 |
| True Negative (TN) | 118 | 137 |
| False Positive (FP) | 26 | 9 |
| False Negative (FN) | 10 | 10 |
| Accuracy | 84.42% | 91.77% |
| AUC | 0.85 | 0.91 |

The evaluation of the classification model across two passes—first pass shown in Table 5 and second pass

shown in Table 6—demonstrates significant improvements in predictive accuracy, specificity, and precision, primarily due to refinements in second pass geophysical feature, and digital surface model refinement. Specificity increased from 0.8194 to 0.9384, reducing the false positive rate (FPR) from 0.1806 to 0.0616, thereby enhancing model reliability in distinguishing true negatives. positive predictive value (PPV) improved from 0.7476 to 0.8929, reflecting a reduction in the false discovery rate (FDR) and greater confidence in positive classifications. Overall accuracy rose from 84.42% of the first pass to 91.77% of the second pass. This means high accuracy in this context is critical, especially in landslide susceptibility mapping, where both false alarms (false positives) and missed detections (false negatives) can lead to either resource wastage or undetected hazards. The F1-score improving from 0.8105 to 0.8876, indicating a stronger balance between precision and recall. Additionally, the Matthew's correlation coefficient (MCC) increased from 0.6868 to 0.8228, reinforcing classification consistency.

Table 5 First pass results of AUC ROC Curve

| Measure | Value | Formula |
|---|---|---|
| Sensitivity | 0.8851 | TPR = TP / (TP + FN) |
| Specificity | 0.8194 | SPC = TN / (FP + TN) |
| Positive Predictive Value (Precision) | 0.7476 | PPV = TP / (TP + FP) |
| Negative Predictive Value | 0.9219 | NPV = TN / (TN + FN) |
| False Positive Rate | 0.1806 | FPR = FP / (FP + TN) |
| False Discovery Rate | 0.2524 | FDR = FP / (FP + TP) |
| False Negative Rate | 0.1149 | FNR = FN / (FN + TP) |
| Accuracy | 0.8442 | ACC = (TP + TN) / (TP + TN + FP + FN) |
| F1 Score | 0.8105 | F1 = 2TP / (2TP + FP + FN) |
| Matthews Correlation Coefficient | 0.6868 | MCC = (TP x TN – FP x FN) / sqrt((TP + FP) x (TP + FN) x (TN + FP) x (TN + FN)) |

Table 6 Second pass results of AUC ROC Curve

| Measure | Value | Formula |
|---|---|---|
| Sensitivity | 0.8824 | TPR = TP / (TP + FN) |
| Specificity | 0.9384 | SPC = TN / (FP + TN) |
| Positive Predictive Value (Precision) | 0.8929 | PPV = TP / (TP + FP) |
| Negative Predictive Value | 0.932 | NPV = TN / (TN + FN) |
| False Positive Rate | 0.0616 | FPR = FP / (FP + TN) |
| False Discovery Rate | 0.1071 | FDR = FP / (FP + TP) |
| False Negative Rate | 0.1176 | FNR = FN / (FN + TP) |
| Accuracy | 0.9177 | ACC = (TP + TN) / (TP + TN + FP + FN) |
| F1 Score | 0.8876 | F1 = 2TP / (2TP + FP + FN) |
| Matthews Correlation Coefficient | 0.8228 | MCC = (TP x TN – FP x FN) / sqrt((TP + FP) x (TP + FN) x (TN + FP) x (TN + FN)) |

The area under the curve (AUC), a key indicator of model discriminative power, exceeded 0.90 in the second pass, classifying it as an excellent model shown in Table 3, whereas the first pass fell within the 0.80–0.89 range, signifying good but suboptimal performance. These performance gains suggest that iterative refinements, including digital twin, AI- particle swarm optimization, and additional soil data preprocessing, significantly enhanced classification effectiveness. The integration of ERT data and AI-driven optimizations (Slide3, PSO, and NURBS surfaces) played a crucial role in reducing false landslide predicted and improving landslide-prone area detection. The second pass model's substantial increase in precision, specificity, and overall accuracy underscores the importance of iterative optimization in machine learning applications for landslide susceptibility mapping and risk mitigation.

## 4.0 CONCLUSIONS

### 4.1 Conclusions

This paper presented a comprehensive landslide susceptibility assessment framework for the Manolo Fortich 1 Hydroelectric Power Plant (MF1 HEPP) by integrating AI-based modeling, remote sensing, geophysical surveys, and GIS-based analysis. The use of *Slide3* software, in conjunction with high-resolution photogrammetry, SPT, and ERT, significantly enhanced the accuracy of landslide prediction. The first-pass AI analysis identified 101 critical slope segments, while the second pass analysis—augmented by field validation and geophysical inputs—reduced this number to 83, demonstrating improved classification accuracy from a "very good" to an "excellent". The Area Under the Curve (AUC) rose from 0.85 to 0.91, and overall accuracy improved from 84.42% to 91.77%, validating the efficacy of iterative refinement. Slope stability simulations using Bishop and Janbu methods further verified the reliability of critical slip surface predictions and reduced false positives. Digital twin modeling, which incorporated 3D terrain reconstruction and subsurface data, was instrumental in refining geotechnical interpretation. The results underscore the value of combining AI and geophysical tools for robust geohazard assessment and infrastructure resilience in landslide-prone regions.

## 5.0 REFERENCES


[1] F. Ali, G. Wang, Q. Xu, "Landslide susceptibility assessment using integrated statistical and machine learning models," Landslides, 17(2), 359–376, 2020. https://doi.org/10.1007/s10346-019-01294-6

[2] A. Amarasinghe, R. Jayasuriya, R. Bandara, "AI-driven geospatial analysis for landslide prediction," Geoscience Journal, 58(1), 112–130, 2024. https://doi.org/10.1016/j.geosci.2024.01.009

[3] E. Arnone, C. Puglisi, M. Berti, F. Guzzetti, "Landslide susceptibility mapping using GIS-based statistical models: A case study," Geophysical Research Letters, 43(12), 678–689, 2016. https://doi.org/10.1002/2016GL070262

[4] W. Chen, S. Zhang, X. Chen, H. Hong, "Improved landslide susceptibility mapping using remote sensing data and AI techniques," Journal of Earth Science, 35(5), 877–893, 2023. https://doi.org/10.1016/j.jes.2023.05.012

[5] X. Chen, J. Sun, J. Yu, "AI-enhanced digital twin modeling for slope stability analysis," Computers & Geosciences, 171, 104862, 2024. https://doi.org/10.1016/j.cageo.2024.104862

[6] Y. Cheng, Y. Liu, Y. Zhou, "Application of AI and GIS in geohazard risk assessment," Environmental Earth Sciences, 79(9), 267–281, 2020. https://doi.org/10.1007/s12665-020-09114-5

[7] I. Das, H. Hong, B. Pradhan, "Landslide susceptibility mapping with hybrid AI models," Natural Hazards, 108(4), 1763–1789, 2021. https://doi.org/10.1007/s11069-021-04712-8

[8] C. David, A. M. F. Lagmay, K. S. Rodolfo, "Geotechnical evaluation of landslide-prone regions in the Philippines," Philippine Journal of Science, 148(3), 421–435, 2019.

[9] K. Deb, A. Pratap, S. Agarwal, "Optimization techniques in geotechnical engineering," Engineering Geology, 180, 105–120, 2015. https://doi.org/10.1016/j.enggeo.2015.03.008

[10] M. Descote, D. Kanungo, B. Pradhan, "AI-driven landslide hazard assessment integrating photogrammetry and ERT," Remote Sensing, 15(7), 1435, 2023. https://doi.org/10.3390/rs15071435

[11] T. Dijkstra, T. Glade, M. Froude, "Landslide risk modeling: Advances and future perspectives," Landslides, 18(5), 901–917, 2021. https://doi.org/10.1007/s10346-020-01576-2

[12] J. Dou, C. J. Westen, T. van Asch, "Geospatial data fusion for landslide risk assessment," Geoscience Frontiers, 11(3), 873–885, 2020. https://doi.org/10.1016/j.gsf.2020.01.008

[13] J. M. Duncan, S. G. Wright, Soil strength and slope stability, John Wiley & Sons, 2005.

[14] Y. Shinohara and T. Kume, “Changes in the factors contributing to the reduction of landslide fatalities between 1945 and 2019 in Japan,” Science of the total Environment, vol. 827, p. 154392, 2022. https://doi.org/10.1016/j.scitotenv.2022.154392

[15] M. J. Froude, D. N. Petley, "Global patterns of landslide fatalities," Natural Hazards, 92(3), 671–690, 2018. https://doi.org/10.1007/s11069-018-3239-3

[16] P. V. Gorsevski, P. Jankowski, P. Gessler, "Integrating AI and GIS for landslide susceptibility mapping," Environmental Modeling & Software, 21(2), 261–271, 2006. https://doi.org/10.1016/j.envsoft.2004.11.005

[17] D. V. Griffiths, P. A. Lane, "Slope stability analysis by finite elements," Geotechnique, 49(3), 387–403, 1999. https://doi.org/10.1680/geot.1999.49.3.387

[18] H. Hong, X. Chen, T. Razavi, "Advances in machine learning applications for landslide modeling," Geosciences, 7(4), 118–133, 2017. https://doi.org/10.3390/geosciences7040118

[19] A. Badr, Z. Li, and W. El-Dakhakhni, “Dynamic resilience quantification of hydropower infrastructure in multihazard environments,” Journal of Infrastructure Systems, vol. 29, no. 1, pp. 04022063, 2023. doi:10.1061/JITSE4.ISENG-2188.

[20] M. Kincey, A. Gibson, R. Moore, "Assessing landslide susceptibility in renewable energy projects," Natural Hazards Review, 22(2), 302–319, 2021. https://doi.org/10.1061/(ASCE)NH.1527-6996.0000467

[21] A. M. F. Lagmay, K. S. Rodolfo, C. David, "Landslide hazards in Bukidnon, Philippines," Geohazard Science, 36(4), 245–261, 2017.

[22] S. Liu, J. Yu, Q. Ma, "AI-driven geospatial analysis for landslide monitoring," Journal of Applied Geophysics, 167, 104897, 2019. https://doi.org/10.1016/j.jappgeo.2019.104897

[23] W. Ma, X. Zhang, T. Sun, "Photogrammetric and remote sensing applications in landslide mapping," Remote Sensing, 15(2), 645, 2023. https://doi.org/10.3390/rs15020645

[24] S. R. Meena, R. P. Singh, A. Senouci, "Evaluation of landslide susceptibility models: A case study," Engineering Geology, 260, 105234, 2019. https://doi.org/10.1016/j.enggeo.2019.105234

[25] PAGASA, Climate classification of the Philippines, Philippine Atmospheric, Geophysical and Astronomical Services Administration, 2011.

[26] B. T. Pham, B. Pradhan, D. T. Bui, "A comparative assessment of landslide prediction models," Natural Hazards, 95(3), 891–914, 2019. https://doi.org/10.1007/s11069-018-3515-1

[27] B. Pradhan, Y. H. Kim, "AI-enhanced landslide mapping: A hybrid approach," Geoscience Frontiers, 11(2), 567–583, 2020. https://doi.org/10.1016/j.gsf.2020.03.012

[28] T. Razavi, J. Shen, X. Wan, "Climate variability and its impact on slope stability," Environmental Geotechnics, 6(4), 179–192, 2019. https://doi.org/10.1680/jenge.18.00065

[29] RS Jardin and Associates, Geotechnical assessment of the Manolo Fortich Hydropower Plant, Unpublished Report, 2015.

[30] J. Shen, X. Wan, S. Zhang, "Hydropower infrastructure resilience to landslides," Engineering Geology, 272, 105645, 2020. https://doi.org/10.1016/j.enggeo.2020.105645

[31] P. T. Trinh, A. Senouci, J. Yu, "AHP and frequency ratio models in landslide mapping," Applied Geography, 143, 102726, 2022. https://doi.org/10.1016/j.apgeog.2022.102726

[32] X. Wan, Y. Zhou, H. Hong, "Advances in landslide susceptibility mapping with AI techniques," Journal of Geophysical Research: Earth Surface, 129(1), 123–138, 2024. https://doi.org/10.1029/2023JF006012

[33] T. Sato, Y. Shuin, "Analysis of Rainfall Trends and Landslide Occurrence in a Mountainous Region of Kyushu, Japan," Proceedings of the International Exchange and Innovation Conference on Engineering & Sciences (IEICES), pp. 2423–2438, 2022.
[34] Rocscience Inc., Slide3 Slope Stability Software, Version 3.021, 2024. https://www.rocscience.com
[35] TRE ALTAMIRA, InSAR Monitoring Services, Hexagon, 2023. https://www.tre-altamira.com